MECHANIKA
TEORETYCZNA
I STOSOWANA
2, 23 (1985)

THE STATE OF EXTENSION OF HONEYCOMB GRID STRIP

TOMASZ LEWIŃSKI

Politechnika Warszawska
Instytut Mechaniki Konstrukcji Inżynierskich

1. Introduction

In the papers [1 - 4] continuum models of elastic hexagonal-type grid plates in plane stress state have been formulated. The following Cosserat-type models have been analysed: two versions resulting from the Woźniak's concept of fibrous Cosserat media and so called $\varkappa$ — models corresponding to Rogula-Kunin's pseudocontinuum description. Moreover a simple asymptotic Horvay's model has been recalled. In the mentioned paper [4] an „a priori" analysis of a range of applicability of the Cosserat-type models has been presented and several hypotheses concerning advantages and disadvantages of the considered differential approaches have been put forward.

The „raison d'etre" of the present work is to elucidate problems concerning accuracy of the Cosserat-type models of dense grid plates. The error analysis is carried out by an example of a grid strip with hexagonal structure in a state of extension. The problem is considered independently by means of analytical approaches based on continuum descriptions as well as via finite element analysis which in the considered case of the grid structure can be treated as an exact method (the errors produced by computer program are neglected). Thus a direct error analysis of the considered continuum models viz. errors of evaluating displacements and rotations of nodes as well as internal forces at the nodes is performed.

The statical problem considered makes it possible to disclose scale effects following here from the coupling of constitutive equations by means of **B** tensor (see [1, 2]). As it has been pointed out in [2 - 4] moduli B and C are determined non-uniquely; they depend upon the choice of a version of Cosserat-type description. These moduli can be treated as small parameters of the theory. Their influence on the final analytical results is various; the aim of the present paper is to analyse this phenomenon and, if it is feasible, to distinguish the best differential approach which induces errors of the smallest values. The presented „a posteriori" analysis allows us to appreciate the hypotheses of the paper [4] which have been obtained by „a priori" analysis of approximation of functions $\hat{\Phi}_{\alpha\beta}(k)$ in k-representation.

2. Formulation of the problem

Consider an infinitely long hexagonal grid strip of the unit thickness in the state of extension, Fig. 2.1. Its height is denoted by L. The rods whose axes constitute hexagons of sides equal to l are connected by rigid nodes. A position of the hexagons with respect to the unloaded boundary lines parallel to the horizontal axis of symmetry is shown in Fig. 2.1. The main nodes (cf. [1 - 4]) are marked by circles. The rods are assumed to be made of isotropic elastic material, Young modulus and Poisson ratio being denoted by E

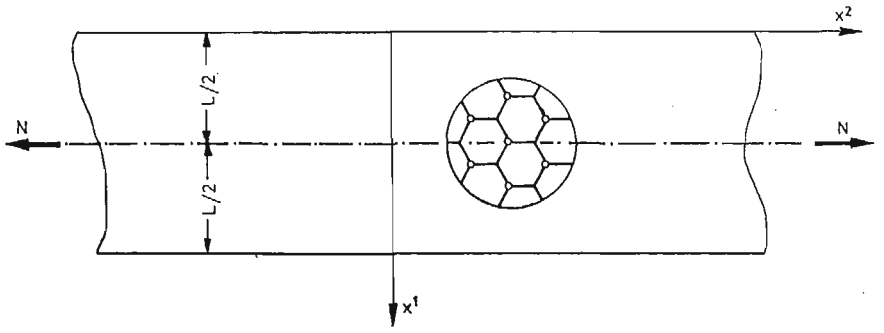

Fig. 2.1

and ν respectively. The heights of rods h (measured in the plane of the strip) are assumed to be constant. The slenderness ratio η of the bars is equal to l^2/h^2. It is assumed that rods are sufficiently slender so as to classical, improved (by taking into account transverse shear deformations) theory of bars can be applied. Moreover it is supposed that all conditions (concerning the loads, density of the grid as well as wavelengths of deformation patterns, see [1 - 4]) being a starting point of the continuum Cosserat-type description are fulfilled here so as to the mentioned mathematical models could be applied.

The displacements and rotations of main nodes are approximated by functions u^α, φ, $\alpha = 1,2$. The state of strain is determined by the tensors $\gamma_{\alpha\beta}$ and $\varkappa_\alpha$ (see [1 - 4]) while the state of stress is expressed by means of the tensors of stresses $p^{\alpha\beta}$ and couple stresses m^α. Elastic properties of the structure are described by means of effective moduli λ, μ, α, B and C.

3. Analytical solutions due to Cosserat-type descriptions

Consider a grid strip of honeycomb structure subjected to stretching forces as in Fig. 2.1. Boundary conditions on the unloaded edges are satisfied exactly whereas stresses in transverse cross-sections are not exactly specified; it is assumed only that both the transverse shear resultant and the resultant moment are equal to zero whereas longitudinal resultant force amounts to N. Owing to the assumed method of fulfilling boundary conditions the one-dimensional state of stress can be achieved. In order to make the functions

$u^\alpha\varphi$ unique a middle point $(L/2, 0)$ is supposed to be fixed. Thus the boundary conditions take the form

$$\begin{gathered} p^{11}(0,y) = 0, \quad p^{11}(L,y) = 0, \\ p^{12}(0,y) = 0, \quad p^{12}(L,y) = 0, \\ m^1(0,y) = 0, \quad m^1(L,y) = 0, \\ \int_0^L p^{22}dx = N, \quad \int_0^L p^{21}dx = 0, \quad \int_0^L [p^{22}(x-L/2)+m^2]dx = 0, \\ u^\alpha(L/2,0) = 0, \quad \varphi(L/2,0) = 0, \quad \alpha = 1,2, \end{gathered} \tag{3.1}$$

where $x^1 = x, x^2 = y$, see Fig. 2.1.

By virtue of one-dimensionality of the problem the functions u^α and φ can be expressed by means of equations linear with respect to the variable y:

$$\begin{aligned} u^1(x,y) &= u(x)+m\cdot y+u_0^1, \\ u^2(x,y) &= v(x)+p\cdot y+u_0^2, \\ \varphi(x,y) &= \varphi(x)+s\cdot y, \end{aligned} \tag{3.2}$$

where m, p, s, u_0^α denote arbitrary integration coefficients.

Deformations associated with the state of displacement read

$$\begin{aligned} \gamma_{11} &= u', \quad \gamma_{22} = p, \quad \gamma_{12} = v'-\varphi-sy, \\ \gamma_{21} &= m+\varphi+sy, \quad \varkappa_1 = \varphi', \quad \varkappa_2 = s, \end{aligned} \tag{3.3}$$

where $(\cdot)' = \partial(\cdot)/\partial x$.

Components of stress and stress couples take the form

$$\begin{aligned} p^{11} &= (2\mu+\lambda)u'+\lambda p+B\varphi', \\ p^{22} &= (2\mu+\lambda)p+\lambda u'-B\varphi', \\ p^{12} &= (\mu+\alpha)(v'-\varphi-sy)+(\mu-\alpha)\cdot(m+\varphi+sy)-B\cdot s, \\ p^{21} &= (\mu+\alpha)(m+\varphi+sy)+(\mu-\alpha)(v'-\varphi-sy)-B\cdot s, \\ m^1 &= C\varphi'+B(u'-p), \\ m^2 &= Cs-B(v'+m), \end{aligned} \tag{3.4}$$

where the constitutive equations of honeycomb grid plate (see [1, 2]) have been applied One-dimensionality of the state of stress implies $s = 0$. The set of equilibrium equations expressed in terms of displacements can be written as follows

$$\begin{aligned} (2\mu+\lambda)u''+B\varphi'' &= 0, \\ (\mu+\alpha)v''-2\alpha\varphi' &= 0, \\ 2\alpha v'-4\alpha\varphi+C\varphi''+Bu''-2m\alpha &= 0. \end{aligned} \tag{3.5}$$

On integrating this system of differential equations and using boundary conditions (3.1) with the aid of strain-displacement (3.3) as well as constitutive (3.4) relations, the components of states of

— displacement

$$u^1(x,y) = u^1(x) = \left[\frac{B^2(\mu+\lambda)(\mu+\alpha)\varepsilon}{2\alpha\mu\lambda(2\mu+\lambda)\operatorname{ch}(\varepsilon L/2)}\operatorname{sh}(\varepsilon(x-L/2)) + \left(x-\frac{L}{2}\right)\right]\zeta$$

$$u^2(x,y) = -\zeta\lambda^{-1}\left[\frac{B(\mu+\lambda)}{\mu\operatorname{ch}(\varepsilon L/2)}\left[\operatorname{ch}\left(\varepsilon\left(x-\frac{L}{2}\right)\right)-1\right]+(2\mu+\lambda)y\right], \tag{3.6}$$

$$\varphi(x,y) = \varphi(x) = -\left[\frac{B(\mu+\lambda)\cdot(\mu+\alpha)\varepsilon}{2\alpha\mu\lambda\operatorname{ch}\dfrac{\varepsilon L}{2}}\operatorname{sh}\varepsilon\left(x-\frac{L}{2}\right)\right]\zeta,$$

— strain

$$\gamma_{11} = \left[\frac{B^2(\mu+\alpha)\cdot(\mu+\lambda)\cdot\varepsilon^2}{2\alpha\mu\lambda\cdot(2\mu+\lambda)\operatorname{ch}(\varepsilon L/2)}\operatorname{ch}\left(\varepsilon\left(x-\frac{L}{2}\right)\right)+1\right]\zeta,$$

$$\gamma_{12} = \left[\frac{(\mu+\lambda)(\mu-\alpha)\cdot B\varepsilon}{2\alpha\mu\lambda\operatorname{ch}(\varepsilon L/2)}\operatorname{sh}(\varepsilon(x-L/2))\right]\zeta,$$

$$\gamma_{21} = \left[\frac{-B(\mu+\lambda)(\mu+\alpha)\varepsilon}{2\alpha\mu\lambda\operatorname{ch}(\varepsilon L/2)}\operatorname{sh}(\varepsilon(x-L/2))\right]\zeta, \tag{3.7}$$

$$\gamma_{22} = -\frac{2\mu+\lambda}{\lambda}\zeta,$$

$$\varkappa_1 = \left[\frac{-B(\mu+\lambda)(\mu+\alpha)\varepsilon^2}{2\alpha\mu\lambda\operatorname{ch}(\varepsilon L/2)}\operatorname{ch}(\varepsilon(x-L/2))\right]\zeta, \quad \varkappa_2 = 0,$$

— and stress

$$p^{11} = p^{12} = 0,$$

$$p^{22} = \left[\frac{B^2(\mu+\lambda)^2(\mu+\alpha)\varepsilon^2}{\alpha\mu\lambda(\lambda+2\mu)\operatorname{ch}(\varepsilon L/2)}\operatorname{ch}\left(\varepsilon\left(x-\frac{L}{2}\right)\right)-\frac{4\mu(\mu+\lambda)}{\lambda}\right]\zeta,$$

$$p^{21} = \frac{-2B(\mu+\lambda)\varepsilon}{\lambda}\,\frac{\operatorname{sh}(\varepsilon(x-L/2))}{\operatorname{ch}(\varepsilon L/2)}\zeta, \tag{3.8}$$

$$m^1 = \frac{2B(\mu+\lambda)}{\lambda}\cdot\left[1-\frac{\operatorname{ch}(\varepsilon(x-L/2))}{\operatorname{ch}(\varepsilon L/2)}\right]\zeta,$$

$$m^2 = \frac{B^2\varepsilon(\mu+\lambda)}{\mu\lambda}\,\frac{\operatorname{sh}(\varepsilon(x-L/2))}{\operatorname{ch}(\varepsilon L/2)}\zeta,$$

are finally found, where

$$\varepsilon = \left[\frac{4\alpha(2\mu+\lambda)\mu}{(\mu+\alpha)[C(2\mu+\lambda)-B^2]}\right]^{1/2}, \quad [\varepsilon] = 1/m,$$

$$\zeta = \frac{0.25N\lambda}{\left[\dfrac{B^2\varepsilon(\mu+\lambda)^2(\mu+\alpha)}{2\alpha\mu(2\mu+\lambda)}\operatorname{th}(\varepsilon L/2)-\mu(\mu+\lambda)L\right]}. \tag{3.9}$$

The quantity ε, being a new „material" constant of the grid, exists due to the energy bounds (5.3), [2]. As it follows from [6] this constant plays essential role in the theory of hexagonal-type grid plates. Patterns of variations of functions (3.6 - 3.8) are presented in Fig. 3.1. Two types of cross-sections are considered: along main nodes ($y_2, y_4, B > 0$) and — intermediate ones ($y_1, y_3, B < 0$).

Note that the function $u^1(x)$ does not depend on sign B so that u^1 displacements of

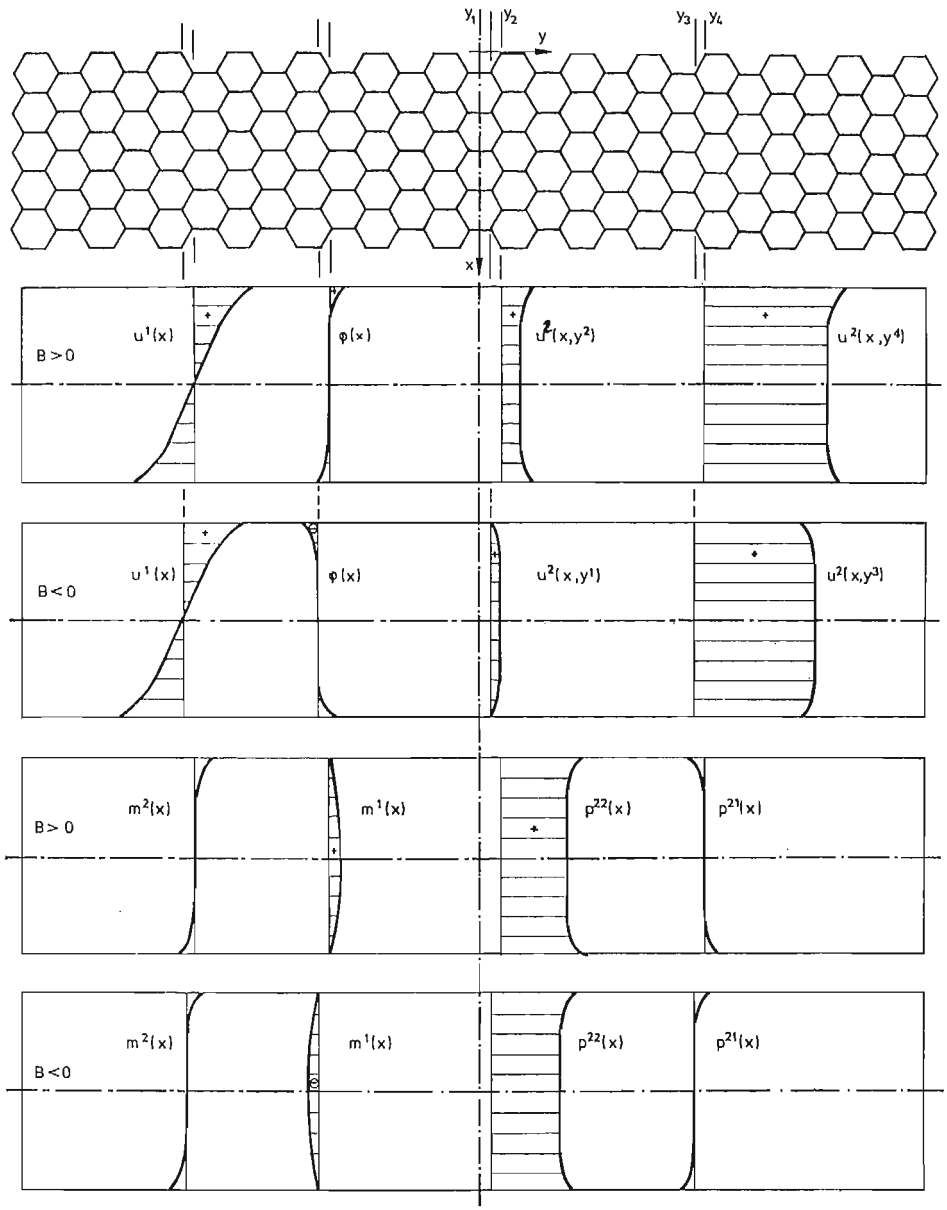

Fig. 3.1

main and intermediate nodes lieing in the same distance from the longitudinal axis of symmetry are identical.

The function u^2 consists of two terms; the first of them depends on sign B whereas the second one is independent of this factor. Thus longitudinal displacements u^2 vary accordingly to the choice of the sections being drawn along main or intermediate nodes (cf. Fig. 3.1).

The function $\varphi(x)$ is proportional to sign B. Thus rotations of main and intermediate nodes, which lie at the same distance from the strip's axis, have same absolute values and opposite signs.

Stresses p^{22} and m^2 do not depend of sign B whereas the stress components p^{21} and m^1 depend upon this factor, cf. Fig. 3.1.

Nonlinear form of the graphs plotted in Fig. 3.1 results from coupling of constitutive equations ($B \neq 0$). The results obtained can be devided into two groups (a) and (b). To the first group these quantities belong which do not vanish if one substitutes $B = 0$; whereas the quantities vanishing in the case of $B = 0$ constitute (b) group. The quantities of (a) type have nonvanishing values along transverse cross-sections. The quantities of (b) type take essential values in edge zones only. These areas which can be treated as effective carriers (i.e. domains where values of functions cannot be neglected in comparison with the values of (a)-type functions) will be called further B-effect zones. Despite apparent imprecision of this definition we do not see any need to give a precise one allthough such a definition can be formulated.

In the subsequent section a numerical test of the theoretically obtained qualitative results and corollaries will be carried out. Moreover the errors induced by Cosserat-type models as well as by asymptotic model (in which $B = C = 0$) will be examined.

REMARK 1

Note that in the problem considered a density of strain energy

$$e = \frac{1}{2}(p^{\alpha\beta}\gamma_{\alpha\beta} + m^{\alpha}\varkappa_{\alpha}) \tag{3.10}$$

does not depend of the choice of main nodes, i.e. of sign B.

REMARK 2

Consider analogous problem of extension of a lattice-type strip of hexagonal structure rotated at an angle $\pi/2$ from the position considered above (as in Fig. 3.1). It can be proved that in this case an assumption of one-dimensionality of a stress state leads to a contradiction; the boundary conditions of the form of (3.1) cannot be fulfilled.

REMARK 3

Examine rotations of the boundary nodes lieing at a distance of $L/2$ from the longitudinal axis of the strip, subjected to stretching stresses $\sigma_{yy} = N/L$, in the limiting case $L \to \infty$ at $l = \text{const}$. By inserting $x = 0$ into $(3.6)_3$ and taking into account that $L \to \infty$ the following formula

$$|\varphi_{\max}/\sigma_{yy}| = \frac{B}{4\mu} \cdot \left[\frac{(2\mu+\lambda)(\mu+\alpha)}{\alpha\mu[C(2\mu+\lambda)-B^2]}\right]^{1/2} \tag{3.11}$$

is obtained. The RHS of Eq. (3.11) involves effective elastic moduli only. In the subsequent section an accuracy of the derived formula will be examined.

4. Numerical analysis by displacement method

The subject of the numerical analysis are plane grid structures A and B (see Fig. 4.1 where the quarters of the structures are shown). The rods are assumed to be made of a steel with Young modulus $E = 2.106 \cdot 10^7$ N/cm^2. Transverse shear deformations of the rods are neglected. Cross-sections of bars are rectangular $1 \times h$ where $h = 1$ cm or $h = 2$ cm. The internode distance l is equal to 10 cm. The both grids are subjected to stretching longitudinal forces $P = 8660.250$ N (cf. Fig. 4.1) hence the mean stress of tension reads

$$\sigma = \frac{P}{l\sqrt{3}/2} = 1000 \text{ N/cm}^2.$$

The state of extension is realized by various ways (exemplary loads are shown in Fig. 4.1). For further analysis only these results are important which do not vary under various statically equivalent systems of loads. The aim of the numerical tests is to create a one--dimensional state of deformation. Thus at some distances from the loaded boundaries of the strip the displacements, strains and stresses (apart from the displacements u^2 parallel to strip's horizontal axis) ought to assume stable values, viz. independent of the distance of the section from the loaded ends. Numerical computations (performed with the aid of the program STRAINS 75, computer ODRA 1305) confirm this supposition which can be interpreted as „discrete analogy" of Saint Venant principle. However, transverse forces in horizontal bars (which occur due to the fact that the strips A and B are of finite length) do not satisfy this condition; their values are not periodical. Nevertheless it should be stressed here that these forces are negligible in comparison with transverse forces in bars whose axes are situated at angles $\pm\pi/3$ from the horizontal symmetry line. Moreover it should be emphasised that periodicity od some quantities occurs in some boundary layer only, e.g. the moments in horizontal bars, reaching the greates values in the vicinity of the unloaded edges, vanish rapidly towards the strip's horizontal axis; the greatest moments only (in B strip-at the first, say, six nodes lieing at the edge) satisfy the desired one-dimensional state of stress condition whereas the other (negligible) values vary at random.

The complete set of numerical results will not be reported; indeed not they are of essential importance here. In the subsequent section selected results will be given together with analytical results obtained by approximate differential models discussed in the paper.

5. Accuracy analysis of the continuum Cosserat-type and asymptotic approaches

This section is devoted to comparison of results analytically obtained in Sec. 3 with results produced by computer analysis (outlined in Sec. 4) of the A and B structures, cf. Fig. 4.1. Such comparison can be carried out, because

a) honeycomb grids A and B satisfy the desired regularity and density conditions,

b) strip-type forms of A and B structures as well as the loads subjected ensure (as it has been pointed out in Sec. 4) a one-dimensional state of stress so that the fundamental assumption of the presented in Sec. 3 analytical approach is fulfilled,

c) deformations of structures vary smoothly except for the B zones lieing at unloaded

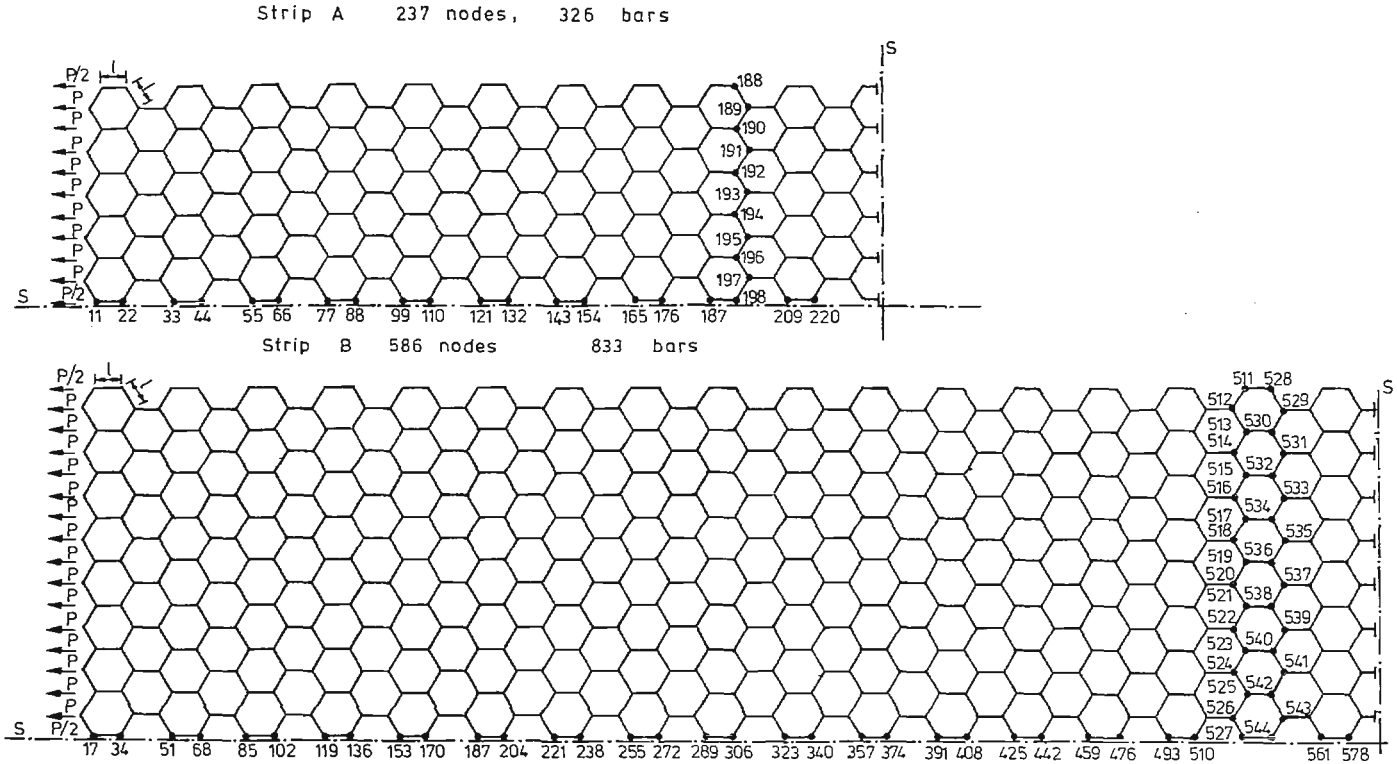
Strip A 237 nodes, 326 bars
P/2
P
l
S
188
189
190
191
192
193
194
195
196
197
198
11 22 33 44 55 66 77 88 99 110 121 132 143 154 165 176 187 209 220
Strip B 586 nodes 833 bars
511 528
512
529
513
530
514
531
515
532
516
533
517
534
518
535
519
536
520
537
521
538
522
539
523
540
524
541
525
542
526
543
527
544
17 34 51 68 85 102 119 136 153 170 187 204 221 238 255 272 289 306 323 340 357 374 391 408 425 442 459 476 493 510 561 578

Fig. 4.1

edges. Thus the mathematical models, based on the assumption that strain energy density depends on the first deformation gradients only, may be applied.

Prior to performing an accuracy analysis of the considered differential models of honeycomb grids, let the effective elastic moduli of the structures A and B, under the assumption of slenderness of bars ($\eta \approx \overline{\eta}$), be computed[1]. The following models are examined: Klemm and Woźniak version (see [2], Sec. 3) with the set of constants $(\lambda, \mu, \alpha, B^{\vee}, C^{\vee})$, second Woźniak — type (II) version (see [2], Sec. 4) with the moduli $(\lambda, \mu, \alpha, B^{\wedge}, C^{\wedge})$ and $\varkappa$ — models (see [4], Sec. 5) leading to the constants $(\lambda, \mu, \alpha\, B^{\circ}, C^{0}_{(\varkappa)})$.

The values of the effective moduli are set up in Table 5.1.

5.1 Approximation of displacements of nodes.

1. Displacements u^1 perpendicular to the strip's horizontal axis

The displacements u^1 of the nodes 188, 189, ..., 198, lieing along the lines perpendicular to the horizontal axis of the strip A (cf. Fig. 4.1), obtained via displacement method (denotations: ∇) as well as by the continuum models, are shown in Fig. 5.1. Relevant graphs of relative errors induced by the latter approaches are plotted in Fig. 5.2. These errors are computed by assuming the results of the displacement method as „exact" ones.

Table 5.1

	l=10cm h[cm]	η	λ[N/cm²]	μ[N/cm²]	α[N/cm²]	$B^{\vee}$[N/cm]	$B^{\wedge}$[N/cm]	B^{0}[N/cm]
a	1	100	583178	11781	1487	58907	29453	51470
b	2	25	1096390	91532	11899	457661	228831	398165

	l=10cm h[cm]	$C^{\vee}$[N]	$C^{\wedge}$[N]	$C^{0}_{(0)}$[N]	$C^{0}_{(1/2)}$[N]	$C^{0}_{(1)}$[N]
a	1	393694	99160	542434	319324	96215
b	2	3081580	793279	4271500	2486630	701747

The „exact" results confirm that behaviour of u^1 function is nonlinear. However, this effect is so unconsiderable that it cannot be shown in Fig. 5.1. It can be noted that the greatest errors are induced by: the zero-order approximation and the unstable ($\varkappa = 1$) model. Apart from this a very good (0.5% - 0.6% error) approximation of u^1 by ($\varkappa = 0$) version is worth emphasising. The second (II) version provides a slightly better results than the first (I) one.

On the basis of computations which are not reported herein it can be stated that in the case of $h = 2$ cm relative errors are greater than in the case of $h = 1$ cm.

An analysis of the u^1 displacements in B strip do not lead to new conclusions. Nevertheless the analysed relative errors are smaller in this case: the (I) version induces ca. 1.4% errors (in A case — 2.3%); the (II) version — 1.07% (in A case — ca. 1.75%); ($\varkappa = 0$) model — ca. 0.34% (in A case — 0.60%); ($\varkappa = 1$) version-ca. 4.4% (in A case — 7.35%). Therefore the more dense a lattice is the better are results.

2. Displacements u^2 parallel to the horizontal symmetry axis

In order to examine u^2 displacements a slightly more complex procedure should be applied since these displacements change their values along the strip's axis. Apart from

[1] For the definition of $\overline{\eta}$, see [2].

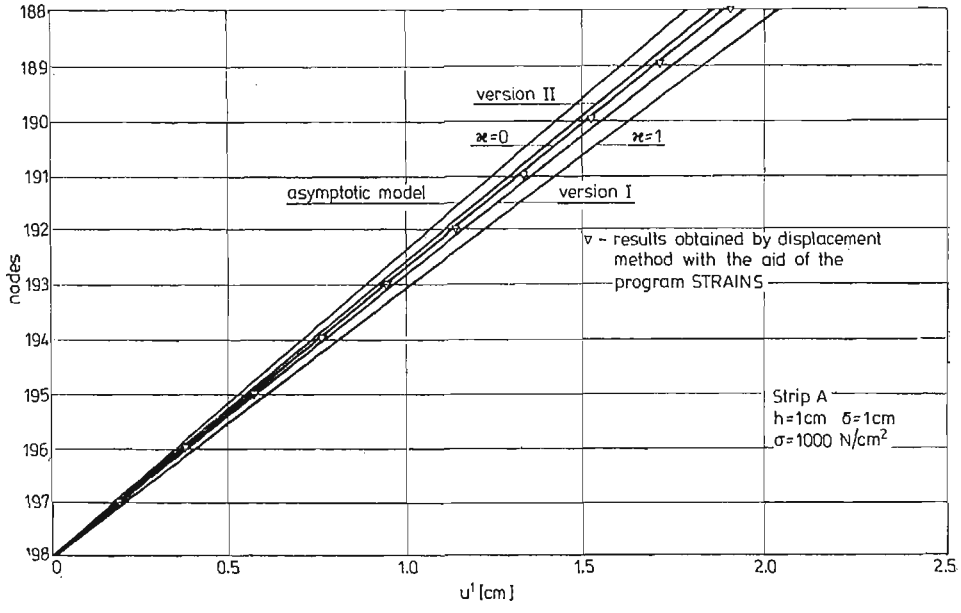
188
189
190
191
192
193
194
195
196
197
198
nodes
0
0.5
1.0
1.5
2.0
2.5
u¹ [cm]
version II
ϰ=0
ϰ=1
asymptotic model
version I
v - results obtained by displacement method with the aid of the program STRAINS
Strip A
h=1cm δ=1cm
σ=1000 N/cm²

Fig. 5.1

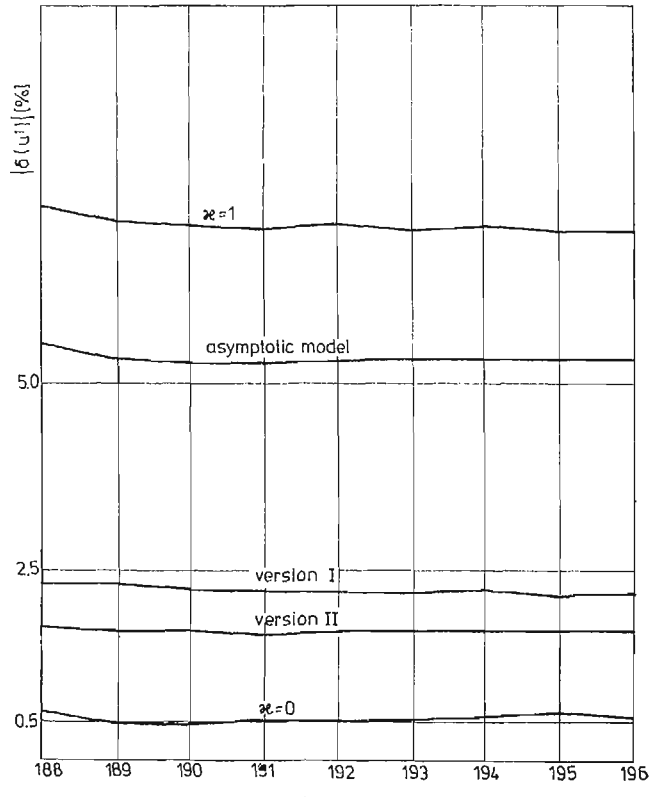
|δ(u¹)| [%]
ϰ=1
asymptotic model
5.0
2.5
version I
version II
ϰ=0
0.5
188
189
190
191
192
193
194
195
196

Fig. 5.2

this an approximation of main and intermediate nodal translations u^2 should be considered separately, see Fig. 3.1.

The displacements u^2 of the nodes 188, ..., 194 (A strip) are shown in Fig. 5.3. Nonlinearities of functions f_1, f_2 interpolating „exact" translations of main and intemediate nodes respectively can be noted, but, on taking into account that their deviations from the straight lines are very small, it could not be shown in Fig. 5.3. However, differential theories produce curvings of u^2 functions much stronger.

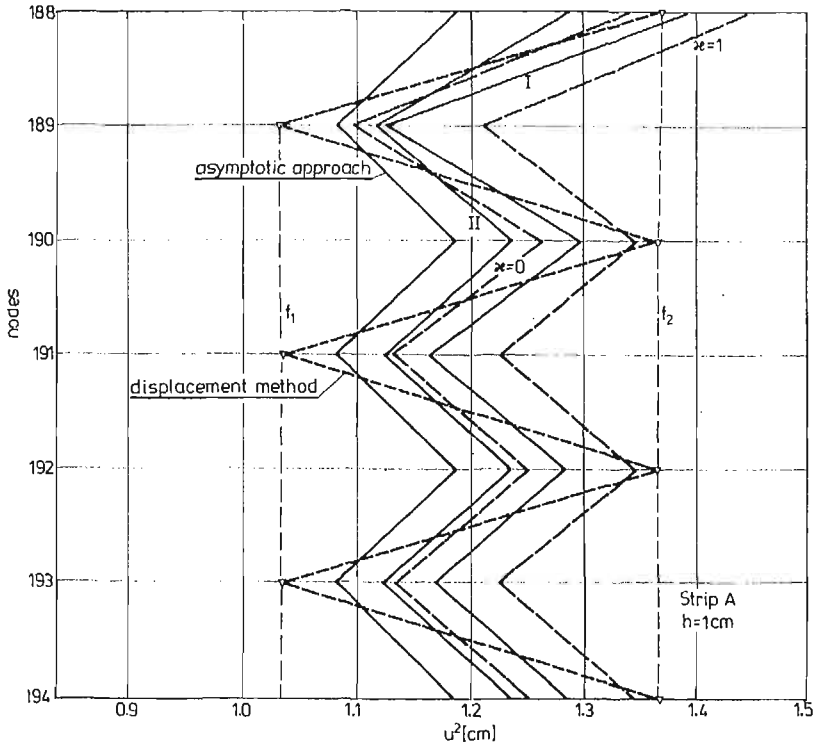

Fig. 5.3

The displacements u^2 of main nodes are approximated in a different manner than analogous displacements of the intermediate nodes. An error analysis of u^2 along cross-sections perpendicular to the horizontal strip's axis proves (cf. Fig. 5.3, see also [5], where appropriate graphs were plotted) that main nodes'displacements are over estimated whereas the intermediate ones are underestimated. Approximation errors of the main nodes'translations u^2 decrease in the edge B-zones while the analogous errors of computing the displacements of the intermediate nodes increase in this zone. A behaviour of relative errors along the horizontal strip axis from the loaded edge to the transverse symmetry axis is worth examining. The relevant graphs are plotted in Figs. 5.4, 5.5. Absolute values of relative errors grow rapidly in the vicinity of the symmetry axis where u^2 tends to zero; then their values go down and again grow at the loaded boundary. Similar diagrams concerning B structure are plotted in Figs. 5.6, 5.7. In this case a stabilization of errors along the strip axis is readily seen.

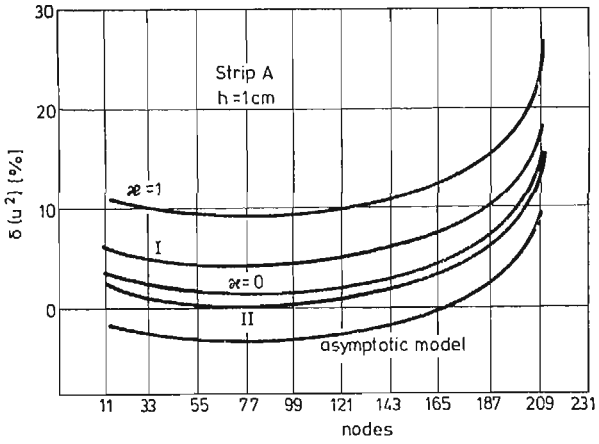

Fig. 5.4

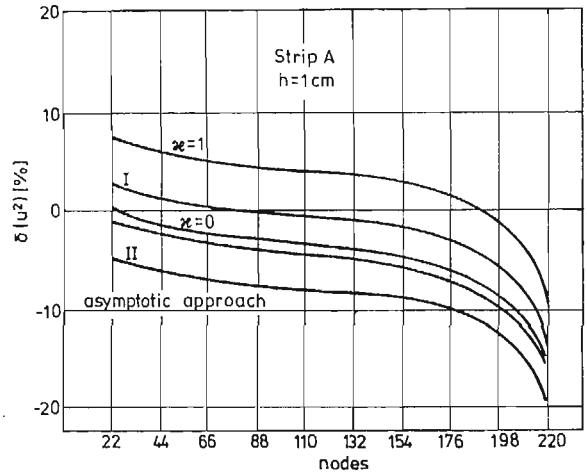

Fig. 5.5

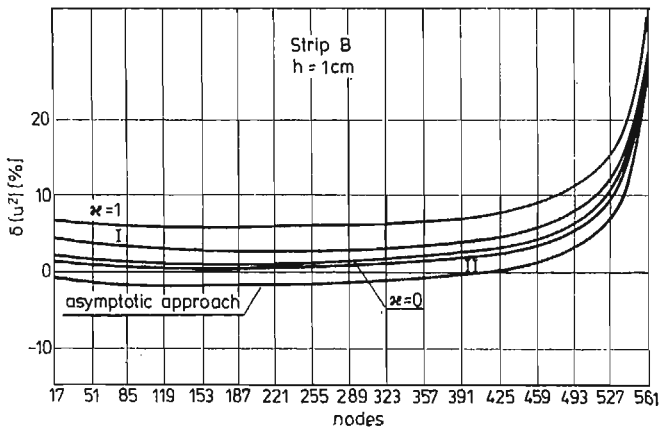

Fig. 5.6

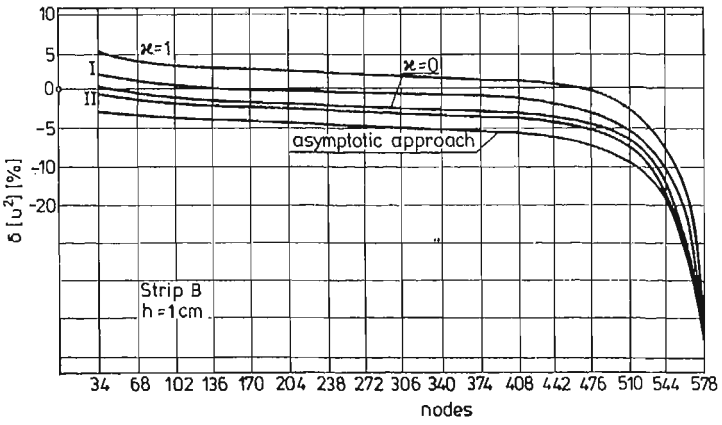

Fig. 5.7

It is worth stressing that approximation errors of displacements of nodes of the B strip are less than analogous errors in the case of the A strip. Thus the errors vary together with the density ratio l/L. Moreover, it was tested that the errors grow if the slenderness ratio η increases.

3. Rotations of nodes φ

Rotations of the nodes lieing along the cross-section lines perpendicular to the strip horizontal axis are set up in Tables 5.2a, 5.2b; the values of rotations are increased 1000 times. The results of the Table 5.2a are shown in Fig. 5.8. A similar behaviour of φ function yields from an analysis of B strip so that the second set of diagrams concerning this structure is omitted here.

Table 5.2 a

Strip A nodes		continuum models					Displacement method
		I	II	ϰ=0	ϰ=1/2	ϰ=1	
188	a	59.613	57.109	43.026	57.117	112.127	41.782
	b	7.667	7.272	5.446	7.325	15.822	5.380
189	a	-21.701	-7.625	-18.242	-18.607	-14.051	-8.452
	b	-2.709	-0.937	-2.275	-2.305	-1.527	-0.994
190	a	7.899	1.020	7.734	6.061	1.761	1.695
	b	0.957	0.121	0.951	0.725	0.147	0.169
191	a	-2.876	-0.136	-3.279	-1.975	-0.221	-0.329
	b	-0.338	-0.016	-0.397	-0.228	-0.014	-0.028
192	a	1.047	0.018	1.390	0.643	0.028	0.085
	b	0.119	0.002	0.166	0.072	0.001	0.007

a) h=1cm, b) h=2cm

Table 5.2 b

Strip B nodes	continuum models					Displacement method
	I	II	ϰ=0	ϰ=1/2	ϰ=1	
528	57.887	56.305	42.232	55.726	106.888	40.927
529	-21.072	-7.518	-17.905	-18.153	-13.395	-8.287
530	7.671	1.004	7.591	5.914	1.676	1.647
531	-2.792	-0.134	-3.218	-1.926	-0.210	-0.324
532	1.016	0.018	1.364	0.628	0.026	0.067

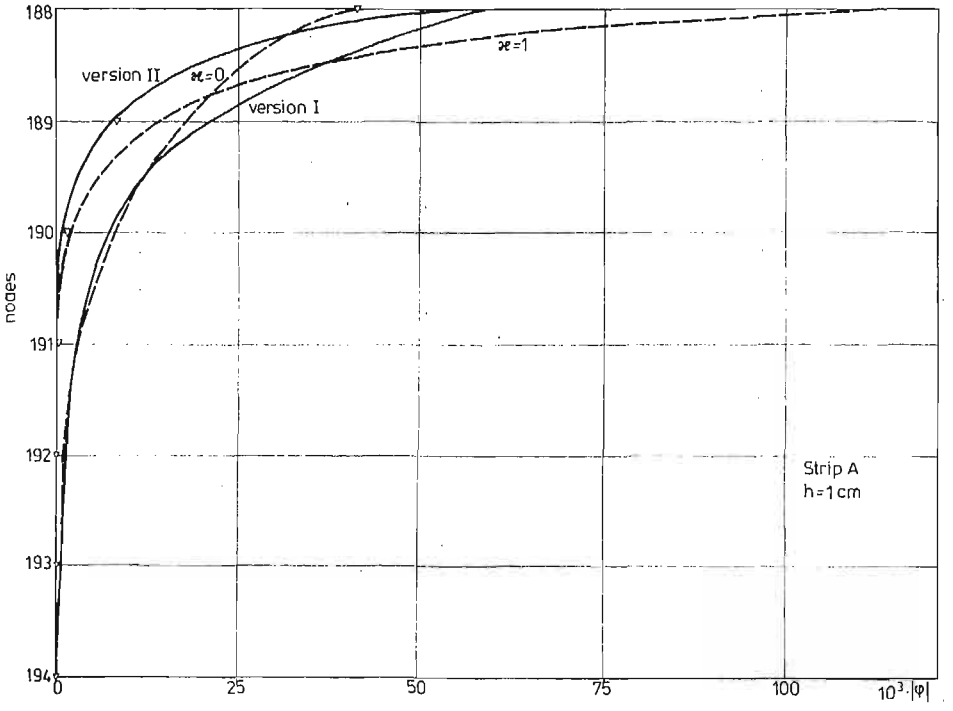

Fig. 5.8

It should be pointed out that continuum description of nodal rotations is qualitatively correct because the all analysed differential theories ensure that:

a) rotations of the main and intermediate nodes lieing at the same distance from the horizontal strip axis have opposite turns since the function φ is proportional to sgnB (cf. $(3.6)_3$) which amounts to -1 and 1 at the intermediate and the main nodes, respectively,

b) the function $|\varphi|$ grows rapidly in the edge B-zones,

c) the B-zone (being a carrier of the essential values of nodal rotations) varies accordingly to the density ratio l/L. In the limiting case when $l/L \to 0$ the B-zone's height vanishes.

The all continuum descriptions produce essential quantitative errors, see Fig. 5.9 where the interpolations of absolute errors (being devided by the maximum value of the rotation of the node lieing on the boundary) are given. A correct evaluation of order of φ is yielded from both the second (II) model and ($\varkappa = 1$) model. The zero-order model does not forecast an existence of nodal rotations in the considered example. Fig. 5.9 discloses that (I), ($\varkappa = 0$) and ($\varkappa = 1/2$) versions bring about greater errors of the rotation description than the most simple asymptotic (zero-order) approach. This fact confirms one of the „a priori" formulated hypothesis following from the approximation analysis of equilibrium equations in k-representation, see [4]. Thus the second (II) version of Woźniak's theory seems to approximate nodal rotations in a best fashion.

A comparison of the results set up in Tables 5.2 leads to a corollary that there is no relation between density of the grid and the approximation errors of φ. Similarly it is

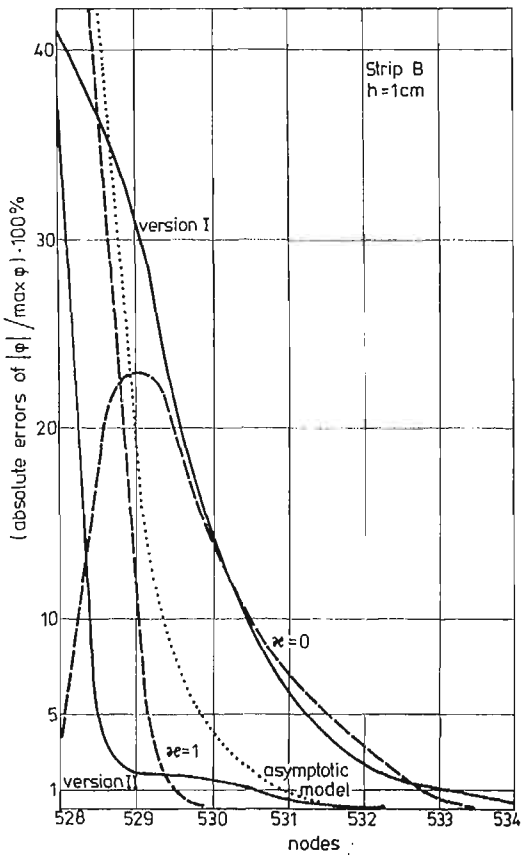

Fig. 5.9

difficult to find a relation between slenderness of lattice rods and an accuracy of analytical solutions.

5.2 Approximation of internal resultant forces. Internal forces in lattice rods can be computed by means of three methods

i) stress method

Consider stress and couple-stress components at the boundary Γ with a unit normal $\mathbf{n}$ and a tangent $\mathbf{t}$ (Fig. 5.10). We have

$$\sigma = \sin^2\alpha \cdot p^{11} + \cos^2\alpha \cdot p^{22} + \sin\alpha\cos\alpha(p^{12}+p^{21}),$$
$$\tau = \sin\alpha\cos\alpha(p^{11}-p^{22}) - \sin^2\alpha \cdot p^{12} + \cos^2\alpha \cdot p^{21},$$
$$m = \sin\alpha \cdot m^1 + \cos\alpha \cdot m^2,$$

where α denotes an angle between $\mathbf{t}$ and x^1 axis.

On the basis of the above formulae the stresses at the sections perpendicular to the bars joint in main nodes of the grid can be found. The longitudinal force, the transverse force and the moment at the nodes are

$$N = \sigma \cdot l\sqrt{3}, \quad T = \tau \cdot l\sqrt{3}, \quad M = m \cdot l\sqrt{3},$$

respectively.

ii) approximate slope-deflection equations' method.

A main idea of the method consists in applying equations which express internal forces in terms of strains, i.e. by means of the formulae (3.3), [2] in (I) version or (4.1), [2], in (II) version. Thus only in the two mentioned cases of continuum descriptions this method can be applied.

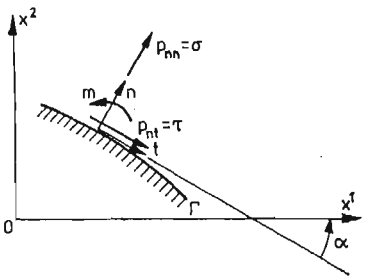

Fig. 5.10

iii) exact slope-deflection equations' method

Internal forces can be calculated by substituting the values of nodal displacements (translations and rotations) into slope-deflection equations well known from the classical theory of bars. However, it occurs that such apparently natural procedure results in completely incorrect outcomes. The appropriate negative examples are presented in [5]. Therefore this method will not be applied in further analysis.

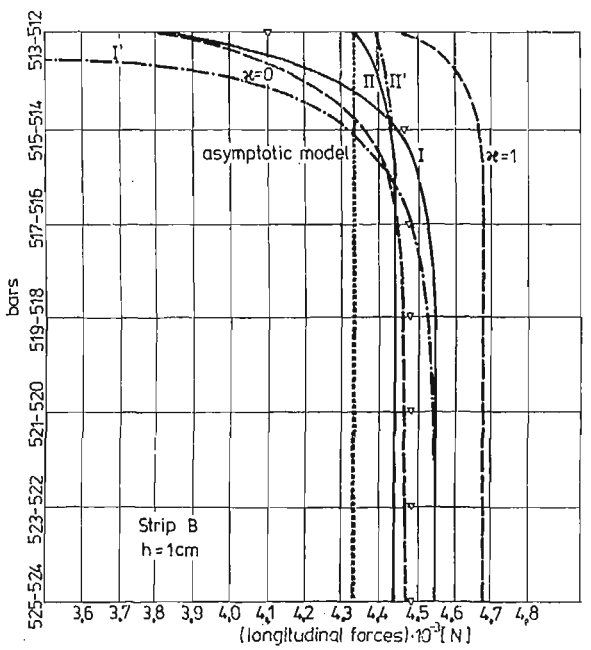

Fig. 5.11

1. Longitudinal forces

Sloping bars. The graphs of functions which interpolate values of longitudinal forces n sloping bars 513 - 512, ..., 524 - 525 (viz. in bars which are inclined from the horizontal symmetry axis of the strip at angles $\pm\pi/3$, see Fig. 4.1) are plotted in Fig. 5.11. By means of a prime (I', II') and the lines —. —. —., the results due to (ii) method are distinguished. The best results are produced by ($\varkappa = 0$) version, the worst — by the asymptotic and unstable ($\varkappa = 1$) models.

Horizontal bars. Appropriate graphs are shown in Fig. 5.12. Similarly to the preceding case the best results yield from (I), (II) and particularly from ($\varkappa = 0$) versions; the worst-are produced by ($\varkappa = 1$) and the asymptotic versions. The latter model does not describe the *B*-effect, of course.

2. Transverse forces

Sloping bars. The functions interpolating transverse forces in bars 513 - 512, ..., 524 - 525 of *B* strip are plotted in Fig. 5.13. The remarks concerning approximations of

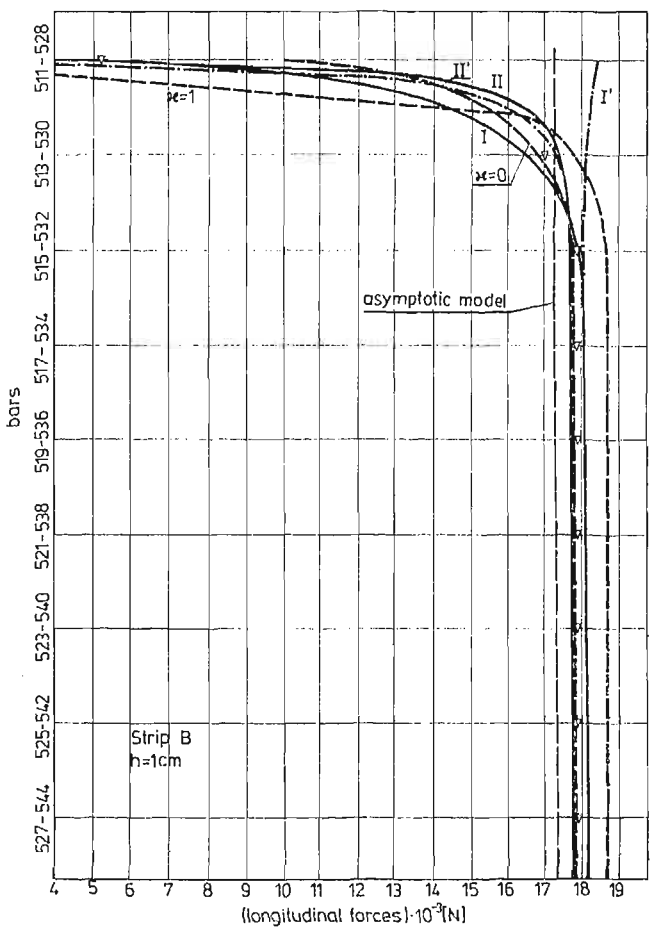

Fig. 5.12

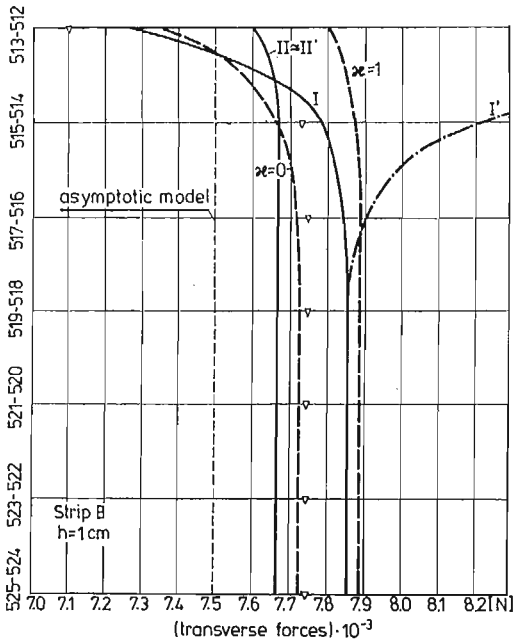

Fig. 5.13

longitudinal forces in sloping bars can be transferred to the considered case of transverse forces. It can be mentioned yet that the method (ii) becomes incorrect in B-zones.

Horizontal bars. Transverse forces in the horizontal bars are equal to zero provided the considered strip is infinitely long. The analytical solution found in Sec. 3 (which is based on the assumption of an one-dimensional stress state) is obtained by virtue of the approximate way of fulfilling the boundary conditions. Specifically the condition $p^{21} = 0$ on the loaded boundary is substituted by an integral expression $(3.1)_8$. Thus $p^{21} \neq 0$ in each Cosserat version whereas the mentioned contradiction does not hold in the zero-order theory where the condition $p^{21} = 0$ is not in contrast to the assumption of onedimensionality of the state of stress. A domain of essential values of p^{21} is a B-effect zone. Thus the solution $T = p^{21} \cdot l\sqrt{3} = 0$ is approximated exactly only by the asymptotic model.

3. Approximation of bending moments

Sloping bars. The functions approximating moments at the nodes of the bars: 513 - 512, ..., 527 - 526 in B strip are plotted in Fig. 5.14. One can pointed out that the second version II', method (ii) provides a very good approximation whereas the ordinary method (i) leads (in the case of the same version) to errors of ca. 50%. Two times increased results of (II) version are shown in Fig. 5.14, the appropriate graph being denoted by $2\,M_{II}$. The coefficient 2 results from the ratio $B^{\vee}/B^{\wedge} = 2$ when $\eta = \bar{\eta}$. The physical interpretation of m^{α} in (II) version especially and also in other versions is not clear and is retained in this paper as open question; some theorems on this problem are formulated in [5].

Horizontal bars. Appropriate graphs standing for moments at nodes of the bars 511 - 528, ..., 527 - 544 in B strip are displayed in Fig. 5.15. The considered moments are

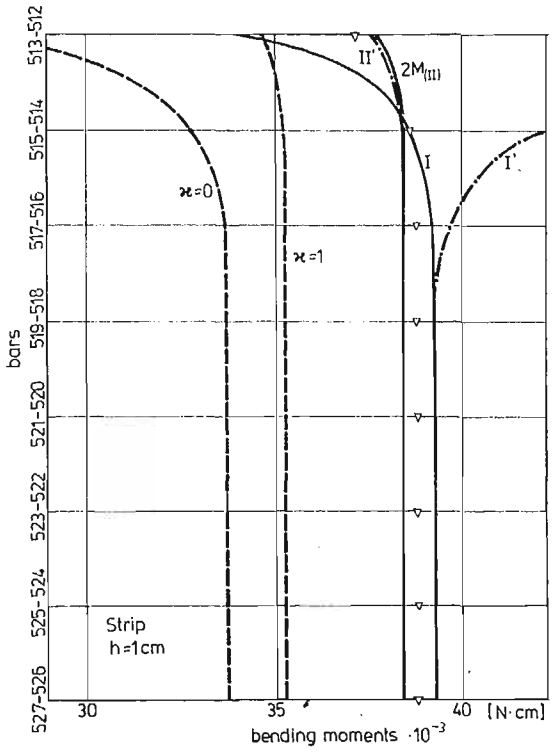

Fig. 5.14

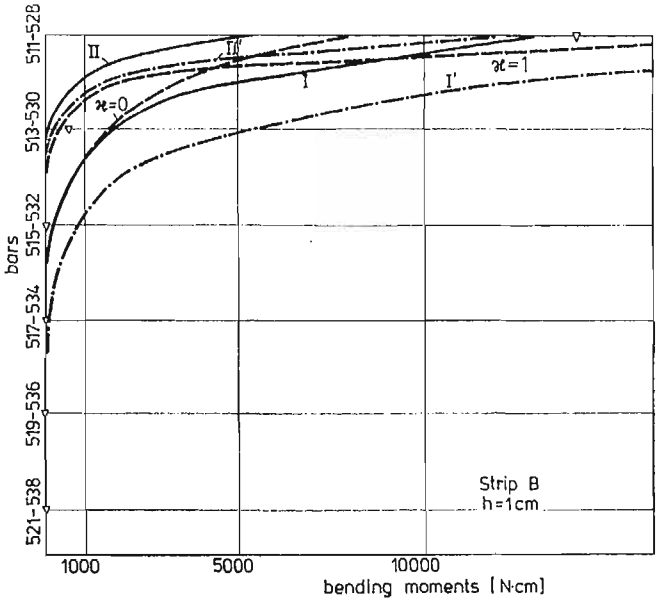

Fig. 5.15

negligibly small comparatively with moments in sloping bars except for the one moment (in the bar 511 - 528) which is of the same order as moments in sloping bars. However, exactly this maximal moment is approximated in the best way, specifically by (I) and (II') methods.

Continuum models supply qualitatively correct description of the bending moments in horizontal bars. However, quantitative errors are considerable; the best results yield from (II') method.

6. Concluding remarks

1) Numerical analysis confirms an existence of B-effect zones which have been predicted previously by the analytical considerations based upon Cosserat-type models (the asymptotic model does not describe this effect). Numerical test proves that the effective height of this zone is evaluated with various degrees of accuracy, the minimal errors yield from the (II) Woźniak's version and from the unstable ($\varkappa = 1$) model. Both analytical considerations and finite element computations show that the B zone's height H varies almost independently of the strip's height L so that a relative height of B zones: H/L decreases if L grows.

2) Quantities characterizing states of stresses and strains of the grid can be divided (as has been done in Sec. 3) into two groups (a) and (b). Computer analysis confirms that such a division is reasonable. Quantities of (a) type take essential values in every point of the strip's cross-sections whereas (b) — quantities take inconsiderable values outside the B — effect domains.

In the B-zones relative errors induced by the continuum models are extreme since exactly in these zones gradients of u^α and φ functions grow rapidly. In these areas a fundamental assumption concerning a smoothness of functions which stand for nodal displacements and rotations is not satisfied.

3) One of the aim of the present paper was to appraise the models which are more complicated than the simplest theory of zero-order accuracy and to answer the obvious question, i.e. whether it is reasonable to use such models. One could get a negative answer, provided in several cases the results produced by asymptotic theory would be more accurate than the results yielded from the models of higher order. The performed analysis proves that such a phenomenon does not hold except for two cases of approximations of the u^2 displacements of main nodes and- the transverse forces in bars horizontal to the strip's axis.

4) Computer analysis confirms that rotations of boundary nodes tend to a non-zero limit φ_{max}^{num} when L grows. In the considered case this limit is ca. 0.041 rad. Theoretical evaluation of this value has been found in Sec. 3, Remark 3, Eq. (3.11). The theoretical results obtained by (I), (II), ($\varkappa = 0$) and ($\varkappa = 1$) versions are displayed below in the Table 6.1.

Table 6.1

	I	II	$\varkappa=0$	$\varkappa=1$
φ_{max}	0.0552	0.0550	0.0409	0.0992

Sufficiently good approximation of the boundary rotation (except for ($\varkappa = 1$) version) is worth emphasising.

5) It has been noted that making of the grid denser implies that errors of approximation of (a) type quantities considerably decrease whereas the errors relevant to (b) type quantities vary inconsiderably and their decreasing has not been observed.

6) An increase in the slenderness of the grid bars makes the evaluation of the displacements u^1 better and the evaluation of the displacements u^2 — worse and has no apparent influence on the approximation of nodal rotations.

A slightly more general accuracy analysis is presented in [5] where errors induced by the so called (III) Woźniak-type model are additionally examined. This version is derived in [5] and has not been a subject of consideration in the papers [1 - 4]. It is sufficient to mention here only that in this model elastic properties of the grid are characterised by the moduli $(\lambda, \mu, \alpha, B^{\vee}, \tilde{C})$ where

$$\tilde{C} = \frac{\sqrt{3}}{3} \cdot \frac{7\eta+4}{\eta+1} \cdot \frac{EJ}{l} \approx \frac{7}{4} \cdot \check{C}$$

in the case of slender grid bars ($\eta \approx \bar{\eta}$). Results produced by this model are resemble to that following from ($\varkappa = 0$) version. The (III) version has not been examined here in order to make an analysis as brief as possible.

References

1. P. KLEMM, Cz. WOŹNIAK, *Dense elastic lattices of hexagonal-type* (in Polish), Mech. Teoret. Stos., **8**, 3, 277 - 293, 1970.
2. T. LEWIŃSKI, *Two versions of Woźniak's continuum model of hexagonal-type grid plates*, Mech. Teoret. Stos., **23**, 3-4, 1984.
3. T. LEWIŃSKI, *Differential models of hexagonal-type grid plates*, Mech. Teoret. Stos., **23**, 3-4, 1984.
4. T. LEWIŃSKI, *Physical correctness of Cosserat-type models of honeycomb grid plates*, Mech. Teoret. Stos., **24**, 1, 1984.
5. T. LEWIŃSKI, *Continuum models of lattice-type hexagonal plates*, *Doctor's Thesis*, Technical University of Warsaw (in Polish) 1983.
6. T. LEWIŃSKI, *Fundamental solutions to the Cosserat-type model of honeycomb grid in a plane-stress state*, Engng. 32, 2. 225-242, 1984.

Резюме

РАСТЯЖЕНИЕ СЕТЧАТОЙ ПОЛОСЫ СО СТРУКТУРОЙ СОТЫ МЁДА

Предметом работы является статический анализ сетчатой полосы (с гексагональной структурой), растяжённой силами, параллельными к её краям. Перемещения узлов и внутренние силы в стержнях анализированы на основе континуальных расчетных моделей типа Коссера: двух версий, вытекающих из общей концепции Возняка и так называемых $\varkappa$ — моделей, предложенных автором в [4], и — при помощи модели Хорвая асимптотического типа. Результаты, вытекающие из расчетных дифференциальных моделей, сравнены с соответствующими результатами, полученными на основе исходной дискретной модели конструкции.

Сформулированы различные предложения, касающиеся полезности и диапазона аппликационности моделей типа Коссера и модели Хорвая.

Streszczenie

ROZCIĄGANIE PASMA SIATKOWEGO O STRUKTURZE PLASTRA MIODU

Przedmiotem rozprawy jest analiza statyczna pasma prętowego o strukturze heksagonalnej rozciąganego siłami równoległymi do jego brzegów. Przemieszczenia węzłów i siły wewnętrzne w prętach badano za pomocą modeli kontynualnych typu Cosseratów: dwóch wersji zgodnych z ogólną koncepcją Woźniaka oraz tzw $\varkappa$ — wersji zaproponowanych przez autora w pracy [4] oraz — za pomocą modelu asymptotycznego Horvaya. Wyniki analityczne porównano z wynikami numerycznymi otrzymanymi metodą przemieszczeń.

Sformułowano szereg wniosków dotyczących użyteczności i zakresu stosowalności modeli typu Cosseratów i modelu Horvaya.

Praca została złożona w Redakcji dnia 30 czerwca 1983 roku